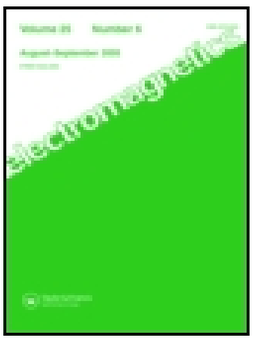

Electromagnetics

ISSN: 0272-6343 (Print) 1532-527X (Online) Journal homepage: http://www.tandfonline.com/loi/uemg20

EVALUATION OF SOMMERFELD INTEGRALS FOR LOSSY HALF-SPACE PROBLEMS

Y. Rahmat-Samii , R. Mittra & P. Parhami

To cite this article: Y. Rahmat-Samii , R. Mittra & P. Parhami (1981) EVALUATION OF SOMMERFELD INTEGRALS FOR LOSSY HALF-SPACE PROBLEMS, Electromagnetics, 1:1, 1-28, DOI: 10.1080/02726348108915122

To link to this article: http://dx.doi.org/10.1080/02726348108915122

EVALUATION OF SOMMERFELD INTEGRALS FOR LOSSY HALF-SPACE PROBLEMS

Y. Rahmat-Samii, *Jet Propulsion Laboratory, Pasadena, CA*
R. Mittra, *University of Illinois*
P. Parhami, *TRW*

ABSTRACT

This paper reviews some of the recent techniques investigated by the authors for numerical, asymptotic and approximate evaluations of the Sommerfeld integrals. Only the summaries of the final formulations are given and their numerical characteristics are illustrated using representative numerical data. Due to space limitations, the discussion in this paper is limited to the cases where both the source and the observation points are above the lossy half-space.

1. INTRODUCTION

Sommerfeld integrals play a fundamental role in the evaluation of the electromagnetic fields due to a current element radiating in the presence of a lossy half-space. The application of the Sommerfeld integrals has been continuously growing in recent years due to a need for accurate analysis of the electromagnetic performance of radiators or scatterers located either above or below a lossy planar half-space. The derivation of these integrals is a rather straightforward electromagnetic problem, and they can easily be obtained from Maxwell's equations by applying the continuity of the tangential fields. However, an efficient and accurate evaluation of the Sommerfeld integrals is a difficult and challenging problem, and has drawn the attention of many prominent researchers during the last two decades.

In its original form, Sommerfeld formulation is an exact integral representation of the solution to the lossy half-space problem. A variety of techniques has been employed to approximate them in a manner which allows an efficient evaluation of the complex integrals. These techniques can be classified as function-theoretic, asymptotic, approximate, numerical, or even combinations of the above. A relatively comprehensive summary of these techniques is given in [1] and more recently in [2]. For the sake of convenience of the reader, we list some of the key references from [2] and [1] in the paragraphs below.

Since the appearance of the original works of Sommerfeld [3], [4], many function-theoretic approaches have been published for different representations of the Sommerfeld integrals, including the series expansions of the same. From the voluminous amount of published data, one may refer to the works of Fock and Bursian [5], [6], Wise [7], [8], Rice [9], Van der Pol [11], Thomas [12], Agrest and Makismov [13], Wait [14], [15], [16], Kochanova and Perov [17] and many others.

Electromagnetics 1:1-28, 1981
0272-6343/81/010001-28$2.25

Methods based on the asymptotic steepest descent path are described in Banos [1], Bleistein and Handelsman [18], Brekhovskish [19], Budden [20], Felsen and Marcuvitz [21], Yokoyama [22], [23], [24], Aboul-Atta, Shafai and Tarnawecky [25] and a number of other publications.

An alternative approach based on the generalized image representations for the Sommerfeld integral has been discussed by Van der Pol [11], Fillipe and Habault [26], Brekhovskish [19], Krylov [27], Brittingham, Miller and Okada [28], Kuo and Mei [29], Chang and Wait [30], and others.

Finally, there has been much interest in developing accurate and efficient numerical techniques based on a variety of purely numerical or semi-analytical numerical methods. Among these, one may refer to Siegel and King [31], Miller, Poggio, Burk and Selden [32], [33], Kong, Shen and Tsang [34], King and Sandler [35], Lytle and Lager [36], Wait and Fuller [37], Haddad and Chang [38], Sarkar [39], McCannon [40], Kuo and Mei [29], Brittingham, Miller and Okada [41], Rahmat-Samii, Parhami and Mittra [42]-[47] and many others. The above list is by no means exhaustive and only demonstrates the wealth of knowledge available in this area.

The objective of the present paper is not to describe all of the above-mentioned approaches but rather to concentrate on the numerical, asymptotic and approximate techniques recently developed by the present authors and to present a coherent review of the same. The details of these techniques can be found in the works of Rahmat-Samii, Parhami and Mittra [42]-[47]. The final formulations and some representative results are included here. Section 2 summarizes the derivation of the Sommerfeld integrals and introduces the notations used in the paper. Section 3 describes an efficient numerical technique for the evaluation of the Sommerfeld integrals based on the numerical integration on the steepest descent path. Section 4 presents the standard reflection coefficient method (RCM) which is obtained from the asymptotic evaluation of the integrals. Section 5 discusses a novel approximate approach which only deals with the Fourier transform of the Sommerfeld integrals and presents its range of validity and limitation. Finally, Section 6 presents numerical results for some representative wire antenna structures over lossy ground.

2. ARBITRARY CURRENT ELEMENT OVER A LOSSY HALF-SPACE (SOMMERFELD INTEGRAL FORMULATION)

The geometry of an arbitrarily oriented current element P_1 over a lossy half-space is depicted in Figure 1. Regions 1 and 2 are characterized by $(\varepsilon_1 = \varepsilon_{1r}\varepsilon_0, \mu_1 = \mu_0)$ and $(\varepsilon_2 = \varepsilon_{2r}\varepsilon_0, \mu_2 = \mu_0)$, respectively, where ε_0 and μ_0 are free-space parameters and $\varepsilon_{2r} = \varepsilon_g - j\sigma_2/(\omega\varepsilon_0)$ is a complex number with the relative dielectric constant ε_g and conductivity σ_2. In addition to the standard Cartesian coordinate system (x,y,z), two spherical coordinate systems (r_1,θ_1,ϕ_1) and (r_2,θ_2,ϕ_2) are also defined in Figure 1 centered about the source point P_1 and its geometrical image point P_2, respectively. Our objective is to determine the field radiated by P_1 at the observation point 0, in the presence of the lossy half-space (region 2).

Starting with Maxwell's equation with the suppressed time convention $\exp(j\omega t)$, one can define the vector potential and apply the Lorentz gauge to express the field equations as:

$$(\bar{\nabla}^2 + k^2)\vec{\Pi} = -(j\omega\varepsilon_0\varepsilon_r)^{-1}\vec{J} \tag{1}$$

$$\vec{H} = j\omega\varepsilon_0\varepsilon_r\bar{\nabla} \times \vec{\Pi} \tag{2}$$

$$\vec{E} = (\bar{\nabla}\bar{\nabla}\cdot + k^2)\vec{\Pi} \tag{3}$$

where $k^2 = \omega^2\mu_0\varepsilon_0\varepsilon_r$. The preceding results are general and valid for both regions 1 and 2. The boundary conditions needed to solve the vector differential Equation (1) can be obtained simply by enforcing the continuity of the tangential $\vec{E}$- and $\vec{H}$-field components at the interface. Without loss of generality, the current source in Figure 1 is assumed to be in the xz-plane (no $\hat{y}$-component), and has the following moment

$$\vec{J} = (\hat{z}\, I_v\, dz' + \hat{x}\, I_h\, dx')\, \delta(x)\, \delta(y)\, \delta(z-h) \quad . \tag{4}$$

Throughout this paper, subscripts v and h will denote the field quantities belonging to the vertical ($\hat{z}$-direction) and the horizontal ($\hat{x}$-direction) current components, respectively. The vector potential expression for region 1 (air), as shown in [43], is derived in the following form:

$$\vec{\Pi} = \Pi_x\, \hat{x} + \Pi_z\, \hat{z} \quad , \tag{5}$$

where

$$\Pi_x = (j\omega\varepsilon_0)^{-1}\, I_h[g(r_1) - g(r_2) + {}_0\Pi_{hx}] \tag{6}$$

$$\Pi_z = (j\omega\varepsilon_0)^{-1}\, I_v[g(r_1) - g(r_2) + {}_0\Pi_{vz}] + (j\omega\varepsilon_0)^{-1}\, I_h\, {}_0\Pi_{hz} \quad , \tag{7}$$

and the free-space Green's function g(r) is conveniently defined as

$$g(r) = \exp(-jk_1 r)/4\pi r \quad . \tag{8}$$

The three vector potential components ${}_0\Pi_{hz}$, ${}_0\Pi_{vz}$, and ${}_0\Pi_{hz}$ in Equations (6) and (7) contain the class of well-known infinite integrals, namely, the Sommerfeld integrals. These integrals can take several forms, as discussed in [1]. In these works, expressions containing the Hankel functions in their integrands are preferred, and, as derived in [43], can be expressed as:

$${}_0\Pi_{vz} = \frac{k_1\kappa}{4\pi j} \int_\Gamma \frac{\sin\xi\cos\xi}{\kappa\cos\xi + \sqrt{\kappa - \sin^2\xi}} H_0^{(2)}(k_1\rho_2 \sin\xi) e^{-jk_1 z_2\cos\xi}\, d\xi \tag{9}$$

$${}_0\Pi_{hz} = \frac{k_1}{4\pi j} \int_\Gamma \frac{\sin\xi\cos\xi}{\cos\xi + \sqrt{\kappa - \sin^2\xi}} H_0^{(2)}(k_1\rho_2 \sin\xi) e^{-jk_1 z_2\cos\xi}\, d\xi \tag{10}$$

and

$${}_0\Pi_{hz} = -\frac{k_1}{4\pi}\cos\phi_2 \int_\Gamma \sin^2\xi\cos\xi \frac{\cos\xi - \sqrt{\kappa - \sin^2\xi}}{\kappa\cos\xi + \sqrt{\kappa - \sin^2\xi}} \cdot H_1^{(2)}(k_1\rho_2 \sin\xi) e^{-jk_1 z_2\cos\xi}\, d\xi \tag{11}$$

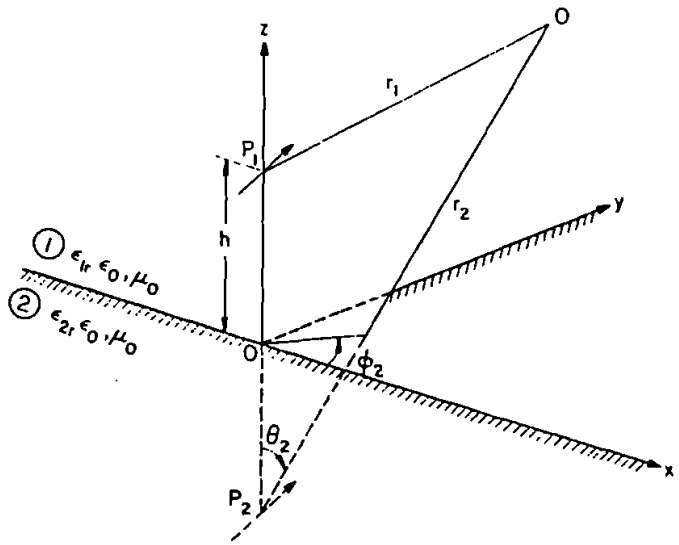

Figure 1. Geometry and the coordinate systems for the current element P_1 radiating over imperfect ground.

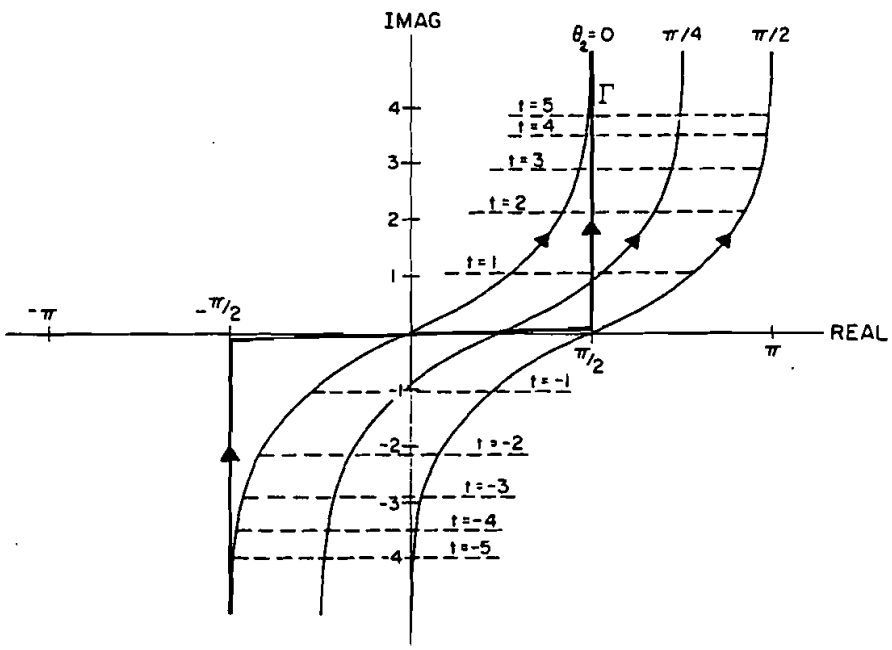

Figure 2. The original integration path Γ and the steepest descent path (SDP) as a function of θ_2.

where path Γ is depicted in Figure 2, on which the condition

$$\mathrm{Im}(\sqrt{\kappa - \sin^2 \xi}) \leq 0 \tag{12}$$

is imposed in order to satisfy the radiation condition. Furthermore, it is noted that $\kappa = \varepsilon_{2r}/\varepsilon_{1r}$ is a complex number.

3. EXACT NUMERICAL INTEGRATION (STEEPEST DESCENT FORMULATION)

Three vector potential components derived in the previous chapter, viz., Equations (9)-(11), cannot be expressed in a closed form as they are the well-known Sommerfeld integrals. In this chapter, an efficient technique is presented for numerically evaluating the aforementioned integrals by deforming the integration contour Γ into the steepest descent path (SDP). This numerical procedure was originally presented by Rahmat-Samii and Mittra [48].

It can be readily shown that all three vector potential components given in (9)-(11) can be expressed in the following general form:

$$u = \frac{1}{4\pi j} \int_{\Gamma} P(\xi) \exp[-jk_1 r_2 \cos(\xi - \theta_2)] d\xi \tag{13}$$

where $P(\xi)$ is a relatively slowly varying function of ξ. The point $\xi = \theta_2$ is a saddle point of Equation (13), and the path Γ can be deformed to a steepest descent path (SDP) by enforcing the condition $\mathrm{Re}[\cos(\xi - \theta_2)] = 1$. (At this point it is assumed that no poles or branch points of $P(\xi)$ are intercepted.) On the SDP, the following convenient change of variable is introduced:

$$\cos(\xi - \theta_2) = 1 - jt^2 \tag{14}$$

where t is a real parameter ranging from $-\infty$ to $+\infty$. Equation (14) can be used to explicitly define the steepest descent path as:

$$\xi_{SDP} = \pm\left[\pi/2 + j \ln(t^2 + j + |t|\sqrt{t^2 + 2j})\right] + \theta_2 \quad ; \; t \gtrless 0 \;, \tag{15}$$

or if one needs to separate the real and the imaginary parts, the following equivalent form can be derived

$$\xi_{SDP} = \pm\left\{\cos^{-1}\left[\frac{-t^2 + \sqrt{t^4+4}}{2}\right] + j \cosh^{-1}\left[\frac{t^2 + \sqrt{t^4+4}}{2}\right]\right\} + \theta_2 \; ; \quad t \gtrless 0 \;, \tag{16}$$

where the inverse cosine function is assumed to be between 0 and $\pi/2$. The SDP can be traced in the ξ-plane, by using Equations (15) or (16) as a function of t and θ_2 (see Figure 2). Applying the change of variable in Equation (14) to the integral expression in Equation (13), we obtain

$$u = \exp(-jk_1 r_2 - j\pi/4)/(2\sqrt{2}\,\pi) \int_{-\infty}^{\infty} Q(t) \exp(-k_1 r_2 t^2)\, dt \tag{17}$$

where

$$Q(t) = \left[P(\xi)\ \sec\frac{\xi - \theta_2}{2}\right]_t = \sqrt{2}\ e^{j\pi/4}(t^2 + 2j)^{-1/2}\ P(\xi)\big|_t \quad . \tag{18}$$

Using the general form obtained in (17), the vector potential expressions in (9)-(11) can be formulated on the steepest descent path as a function of the real variable t, namely,

$$0^{\Pi}_{vz} = \int_{-\infty}^{\infty} \frac{\kappa R_0(t)}{[\kappa \cos\xi + \sqrt{\kappa - \sin^2\xi}]_t} \exp(-k_1 r_2 t^2)\ dt \tag{19}$$

$$0^{\Pi}_{hx} = \int_{-\infty}^{\infty} \frac{R_0(t)}{[\cos\xi + \sqrt{\kappa - \sin^2\xi}]_t} \exp(-k_1 r_2 t^2)\ dt \tag{20}$$

$$0^{\Pi}_{hz} = -j\cos\phi_2 \int_{-\infty}^{\infty} R_1(t)\left[\sin\xi\ \frac{\cos\xi - \sqrt{\kappa - \sin^2\xi}}{\kappa\cos\xi + \sqrt{\kappa - \sin^2\xi}}\right]_t \cdot \exp(-k_1 r_2 t^2)\ dt \tag{21}$$

where

$$R_i(t) = (2\pi)^{-1} k_1 \exp(-jk_1 r_2)(t^2 + 2j)^{-1/2}[\sin\xi\cos\xi\exp(jk_1\rho_2\sin\xi)]_t \cdot H_i^{(2)}(k_1\rho_2\sin\xi)\big|_t \quad ;\ i = 0,1 \quad , \tag{22}$$

$H_i^{(2)}$ is the Hankel function of the i^{th} order and of second kind, and ξ is expressed as a function of t in Equation (15). The relations expressed in Equations (19)-(21) are exact if no poles or branch points are intercepted under the path deformation. It should also be noted that the apparent singularity of the Hankel functions at $\theta_2 = 0$ in the Sommerfeld integrals is overcome by the remaining terms in the integrands [43].

From the integral expressions in (19)-(21), it can be deduced that for large $k_1 r_2$ the effective integration interval is small and contains relatively few oscillations (see Figure 3). Fortunately, at lower frequencies (smaller $k_1 r_2$), the oscillatory terms present in the integrals are scaled accordingly and, even though the effective integration interval increases, the number of oscillations in the integrand does not increase appreciably (Figure 4). This fact allows one to integrate Equations (19)-(21) numerically by employing an efficient Gaussian quadrature integration routine for a wide range of parameters. Later in this paper, the efficiency and the accuracy of the above numerical integration procedure are demonstrated and compared to other available techniques.

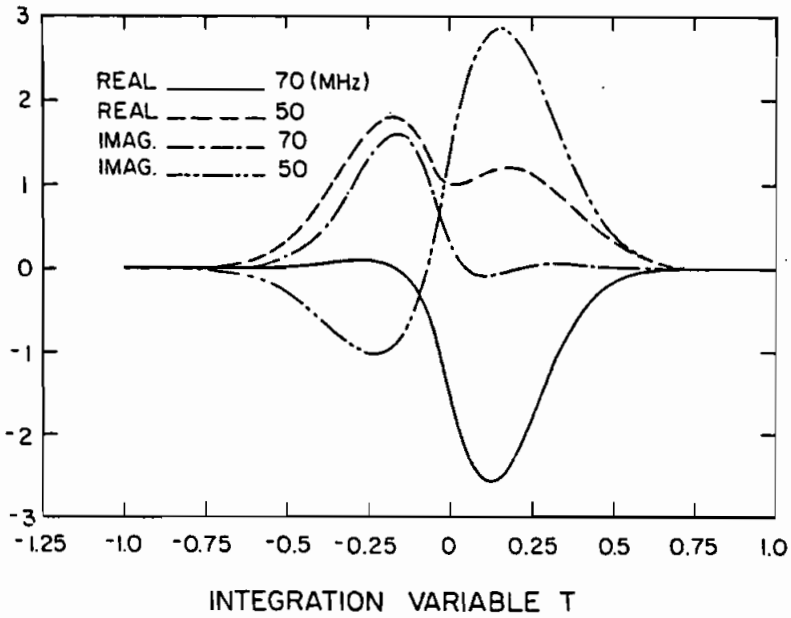

Figure 3. High frequency examples of the ${}_0\Pi_{hx}$ integrand. For these cases, $\theta_2 = 5°$, h = 5m, $\varepsilon_g = 10$, and $\sigma = .01$ mhos/m.

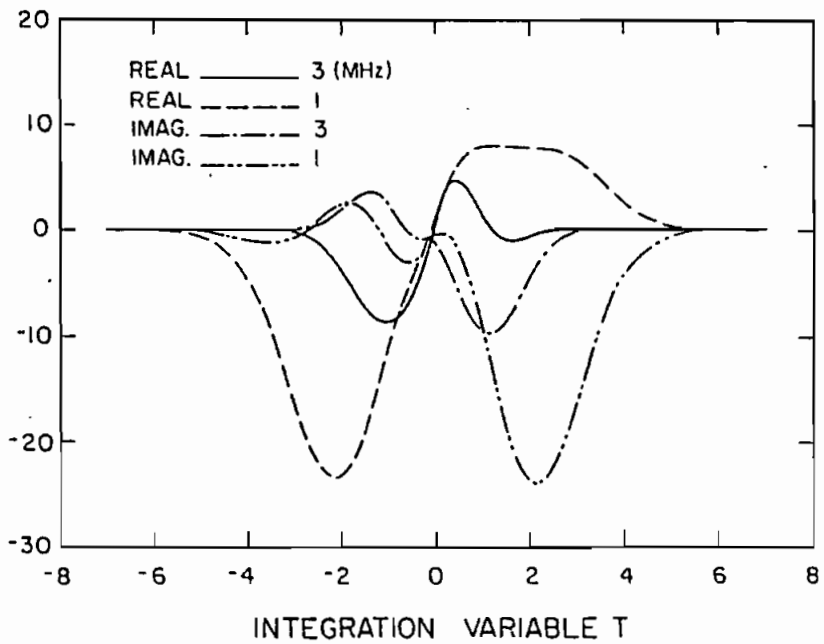

Figure 4. Low frequency examples of the ${}_0\Pi_{hx}$ integrand. For these cases, $\theta_2 = 5°$, h = 5m, $\varepsilon_g = 10$ and $\sigma = .01$ mhos/m.

3.1 Branch-Cut Contribution

The expressions derived in the previous section are valid only when no singularities are intercepted during the steepest descent path deformation. In order to locate the poles and the branch points, one must consider the following physical constraints:

a) $0 \leq \theta_2 < \pi/2$, since Equations (19)-(21) are valid only for observation points above ground;
b) $\mathrm{Re}(\kappa) \geq 1$ and $\mathrm{Im}(\kappa) \leq 0$, since $\kappa = \varepsilon_g - j\sigma/(\omega\varepsilon_0)$;
c) $-\frac{\pi}{2} < \mathrm{Re}(\xi) < \pi$ on the SDP (see Figure 2).

Condition (12) is used to define an upper- and a lower-Riemann sheet in the ξ-plane in which this condition is satisfied in the upper, and violated in the lower, sheet.

Equations (19)-(21) have the same branch points satisfying

$$\kappa - \sin^2 \xi_b = 0 \quad . \tag{23}$$

If one considers the physical constraints discussed earlier, only the following two branch-point solutions are of importance (see Figure 5):

$$\xi_b = \pi/2 \pm j\, \mathrm{Ln}(\sqrt{\kappa} + \sqrt{\kappa - 1}) \quad . \tag{24}$$

The corresponding branch cuts of Equation (24) which satisfy the relation

$$\mathrm{Im}(\sqrt{\kappa - \sin^2 \xi}) = 0 \quad , \tag{25}$$

as depicted in Figure 5, are the boundaries through which the integration path will travel to and from the two Riemann sheets defined earlier. Since the steepest descent path defined in Equation (15) is independent of κ, one can easily demonstrate that for $0 \leq \theta_2 < 90°$ only the branch point with the upper sign can be captured by the SDP deformation (Figure 6). Therefore, one can allow the SDP to enter the lower sheet only when the lower branch cut, corresponding to the lower sign of Equation (24), is intercepted, since the path will always intercept the lower cut at an additional point forcing it to return to the upper Riemann sheet (see Figure 6). A branch-cut integration, however, is performed around the upper-branch cut whenever it is intercepted in order to remain in the proper sheet. The branch cut in the upper-half plane as a function of a positive real parameter β can be expressed as

$$\xi_{bc} = \pi/2 + j\, \mathrm{Ln}(\sqrt{\kappa - \beta^2} + \sqrt{\kappa - 1 - \beta^2}) \quad , \tag{26a}$$

or, equivalently,

$$\sin \xi_{bc} = \sqrt{\kappa - \beta^2} \tag{26b}$$

$$\cos \xi_{bc} = -j\sqrt{\kappa - 1 - \beta^2} \quad . \tag{26c}$$

By applying the change of variable in Equation (26) to the Sommerfeld integrals expressed in (9)-(11) and integrating around the branch cut, the following contributions are obtained:

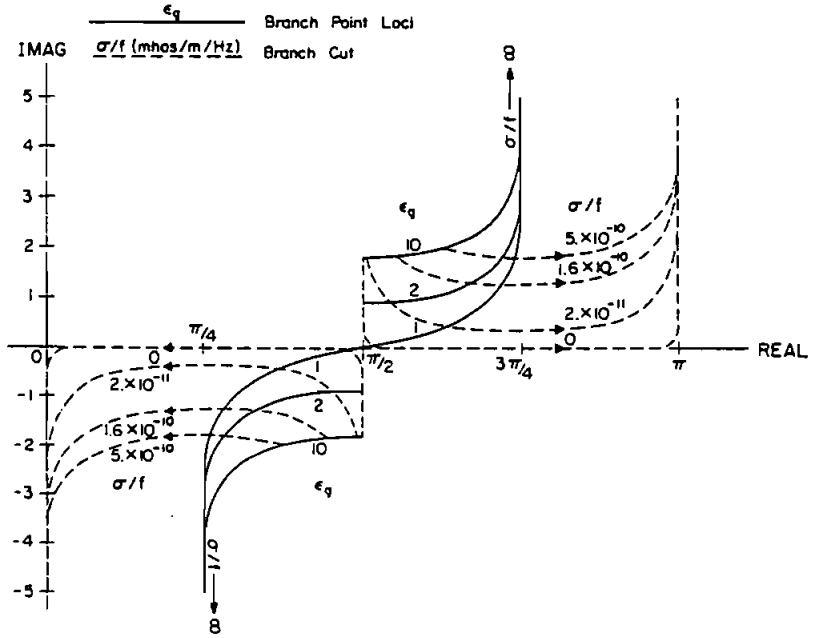

Figure 5. Branch point and branch cut loci as a function of ground parameters ϵ_g and σ/f.

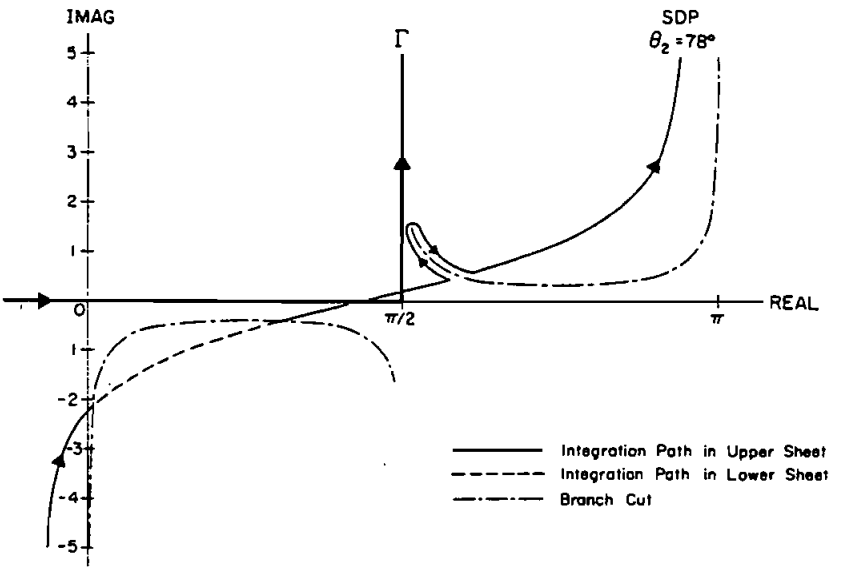

Figure 6. The correct SDP when branch cuts are intercepted. For this case, $\epsilon_g = 10$, and $\sigma/f = 2 \times 10^{-11}$ mhos/mHz.

$$0\Pi_{vz}\Big|_{bc} = k_1\kappa(2\pi j)^{-1}\int_0^{\beta_1}\frac{\beta^2}{\kappa^2\cos^2\xi_{bc}-\beta^2}H_0^{(2)}(k_1\rho_2\sin\xi_{bc})$$
$$\cdot\exp(-jk_1z_2\cos\xi_{bc})\,d\beta \tag{27}$$

$$0\Pi_{hx}\Big|_{bc} = k_1(2\pi j)^{-1}\int_0^{\beta_1}\frac{\beta^2}{\kappa-1}H_0^{(2)}(k_1\rho_2\sin\xi_{bc})\exp(-jk_1z_2\cos\xi_{bc})\,d\beta \tag{28}$$

$$0\Pi_{hz}\Big|_{bc} = k_1(2\pi)^{-1}\cos\phi_2\int_0^{\beta_1}(1+\kappa)\frac{\beta^2}{\kappa^2\cos^2\xi_{bc}-\beta^2}$$
$$\cdot\sin\xi_{bc}\cos\xi_{bc}H_1^{(2)}(k_1\rho_2\sin\xi_{bc})\exp(-jk_1z_2\cos\xi_{bc})\,d\beta\,, \tag{29}$$

where $\beta = \beta_1$ is the crossing point of the branch cut and the SDP in the ξ-place. By expanding Equation (14) and by employing the relations in (26), the following conditions are obtained for β_1

$$\sin\theta_2\,\mathrm{Re}(A) + \cos\theta_2\,\mathrm{Im}(B) = 1 \tag{30a}$$

$$[-\sin\theta_2\,\mathrm{Im}(A) + \cos\theta_2\,\mathrm{Re}(B)]^{1/2} = t_1 \tag{30b}$$

where the complex numbers A and B are defined as

$$A = \sqrt{\kappa-\beta_1^2}\;;\quad \mathrm{Re}(A)\geq 0\;,\quad \mathrm{Im}(A)\leq 0 \tag{31a}$$

$$B = \sqrt{\kappa-1-\beta_1^2}\;;\quad \mathrm{Re}(B)\geq 0\;,\quad \mathrm{Im}(B)\leq 0\;. \tag{31b}$$

In (30), $t = t_1$ defines the point at which SDP, corresponding to the observation angle θ_2, intercepts the branch cut of Equation (26) at $\beta = \beta_1$. After some algebraic manipulations, Equation (30a) can be further simplified to

$$\theta_2 = \sin^{-1}([\mathrm{Re}^2(A)+\mathrm{Im}^2(B)]^{-1/2}) - \tan^{-1}\left[\frac{\mathrm{Im}(B)}{\mathrm{Re}(A)}\right] \tag{32}$$

from which θ_{min}, the observation angle at which SDP will pass through the branch point, can be computed by setting $\beta_1 = 0$. Note that θ_{min} is only a function of κ. Therefore, whenever the observation angle θ_2 satisfies the condition

$$\theta_2 > \theta_{min}\;, \tag{33}$$

the branch-cut contributions in (27)-(29) are to be added to their respective SDP vector potential formulations expressed in (19)-(21).

It should be pointed out that once the condition (33) is met, the branch-cut integration limit β_1 can be computed numerically by iterating on Equation (32). Also, because of the branch-cut interception, the SDP integrand will be discontinuous at point $t = t_1$, which is readily computed by substituting the value of β_1 into (30b).

Fortunately, in many cases, the branch-cut contributions are orders of magnitude smaller than the SDP integral value and can be ignored [49]. Therefore, it is necessary to introduce a condition for which one can ignore the branch-cut integration and thereby compute the vector potentials more efficiently. This task can be accomplished by initially considering the $\exp(-k_1 r_2 t^2)$ term present in all three vector potential integrands shown in (19)-(21). If no poles are present on or near the contour, a finite integration in the interval

$$|t| \leq \left[\frac{9}{k_1 r_2}\right]^{1/2} \tag{34}$$

will result in an error on the order of 0.01% as compared to the full infinite integration. By examining the branch-cut loci (Figure 5) and the SDP behavior (Figure 2) in the ξ-plane, an assumption can be made which states that if the branch cut intercepts the SDP inside the finite integration interval defined in (34), then the branch-cut contribution is not negligible. Or equivalently, the branch-cut contribution requires an additional condition, namely,

$$t_1 \leq t_{max} = 3(k_1 r_2)^{-1/2} \tag{35}$$

where $t = t_1$ is the SDP and the branch-cut intercept defined earlier. More details on this subject are given in [47].

Figure 7 compares the results obtained by our integration techniques for a horizontal antenna over lossy ground with those of Miller et al. [32]-[33]. Our results, which are obtained by applying pulse basis and delta matching in a finite difference sense to the method of moment formulation [50], agree quite convincingly with those in references [32]-[33]. It is important to note that only for larger θ_2 and smaller σ/f values does the branch-cut contribution become significant (see Figure 7) and accurate integration of Equations (27)-(29) becomes necessary. The branch-cut integration, when needed, can be performed much faster than those for Equations (19)-(21), and does not slow down the overall process appreciably.

3.2 Pole Contribution

Unlike the branch points, which exist in all three of the vector potential components, the poles only exist in the z-component of the vector potentials, viz., ${}_0\Pi_{hz}$ and ${}_0\Pi_{vz}$, and satisfy the relation

$$\kappa \cos \xi_p + \sqrt{\kappa - \sin^2 \xi_p} = 0 \quad . \tag{36}$$

Again, by considering the physical constraints discussed at the start of the previous section, only the following two poles need to be considered

$$\xi_p = \pi/2 \pm j[\mathrm{Ln}(\sqrt{\kappa} - j) - \mathrm{Ln}(\sqrt{\kappa + 1})] \quad . \tag{37}$$

Fortunately, one can verify that for $0 \leq \sigma/f < \infty$, $0 \leq \theta_2 < 90°$, and by considering the correct Riemann sheets (see Figure 6), the poles in Equation (37) are not captured by the SDP and the residue contribution is not needed. However, under extreme circumstances, i.e., $\theta_2 \doteq 90°$ and small ε_g, a pole can come close to the SDP. In this case, a higher-order Gaussian quadrature

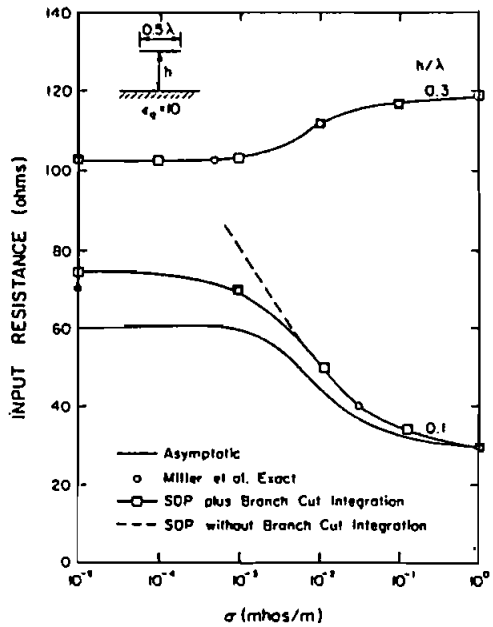

Figure 7. Comparison results for a 0.5λ dipole antenna radiating over lossy ground.

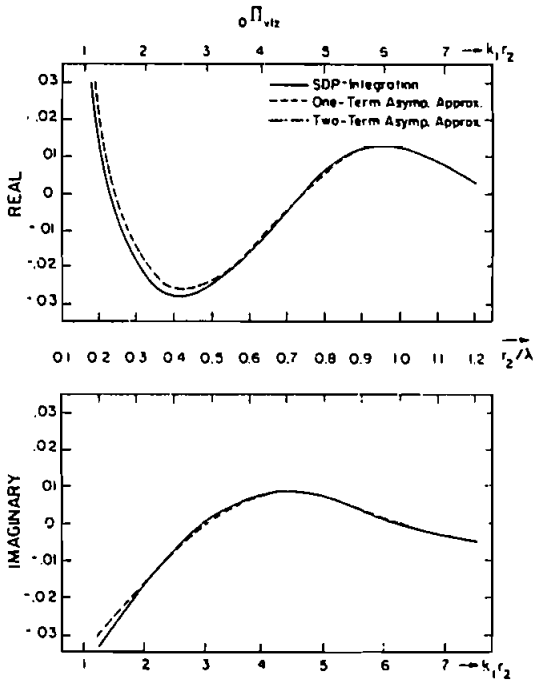

Figure 8. Comparing the SDP integration with the RCM asymptotic expansion of $_0\Pi_{vz}$. For this case, frequency = 30 mHz, $\theta_2 = 10°$, $\phi_2 = 0$, $\varepsilon_g = 10$ and $\sigma = .01$ mhos/m.

integration routine will be required and possibly the effective integration interval in (34) should be expanded.

4. ASYMPTOTIC APPROXIMATION OF THE SOMMERFELD INTEGRALS

As $k_1 r_2$ in the general formulation (17) becomes larger and larger, one can effectively replace Q(t) by its functional value at the saddle point and then apply the standard SDP asymptotic evaluations to find

$$Q(t) \sim P(\theta_2) \tag{38a}$$

$$u \sim (j8\pi k_1 r_2)^{-1/2} \exp(-jk_1 r_2)\, P(\theta_2) \quad . \tag{38b}$$

Applying the latter results to the vector potential expressions (19)-(21), one can derive the following well-known Fresnel Reflection Coefficient approximation:

$$0^{\Pi}_{vz} = \frac{2\kappa \cos\theta_2}{\kappa \cos\theta_2 + \sqrt{\kappa - \sin^2\theta_2}} \exp(-jk_1 r_2)/4\pi r_2 + 0(k_1 r_2)^{-2} \tag{39}$$

$$0^{\Pi}_{hx} = \frac{2 \cos\theta_2}{\cos\theta_2 + \sqrt{\kappa - \sin^2\theta_2}} \exp(-jk_1 r_2)/4\pi r_2 + 0(k_1 r_2)^{-2} \tag{40}$$

$$0^{\Pi}_{hz} = 2 \cos\phi_2 \sin\theta_2 \cos\theta_2 \frac{\cos\theta_2 - \sqrt{\kappa - \sin^2\theta_2}}{\kappa \cos\theta_2 + \sqrt{\kappa - \sin^2\theta_2}}$$

$$\cdot \exp(-jk_1 r_2)/4\pi r_2 + 0(k_1 r_2)^{-2} \quad . \tag{41}$$

The above Reflection Coefficient Method (RCM) expressions have been extensively used in the literature for high-frequency antenna applications ($k_1 r_2$ large) with surprisingly accurate results. This success has been mainly due to the fact that for observation points away from the interface, the remaining vector potential components present in (6) and (7) tend to dominate over the RCM components thereby reducing the net error in the total vector potential values computed. It is worthwhile to mention that higher-order asymptotic terms can also be constructed in a relatively straightforward fashion [1], [43], [47]. An error of 5% or less can be expected in the RCM vector potential components shown in (39)-(41) when

$$k_1 r_2 \geq 10 \quad , \tag{42}$$

and as long as the branch-cut conditions given in the previous section are not violated. Figure 8 compares the RCM and the exact integration results of one of the vector potential components for a typical half-space as a function of $k_1 r_2$.

The computing time, of course, is the main reason why the RCM approximations are used whenever possible. For example, the execution time on a Cyber 175 computer for computing the three vector potentials is ≃ 1 msec for the RCM approximation and as high as 50-100 msec for the SDP integration technique presented in this work. It should be pointed out, however, that the SDP integration is an order of magnitude faster than many of the previously reported integration techniques, making it more suitable for a much wider range of low-frequency applications.

5. AN APPROXIMATE ANALYTIC-NUMERICAL TECHNIQUE FOR EVALUATING THE SOMMERFELD INTEGRALS

The conventional approach for analyzing antenna problems over lossy ground involves repeated evaluations of the Sommerfeld integrals appearing in the expressions for the vector potentials, viz., Equations (19)-(21). Even though the SDP procedure discussed in Section 3 is an efficient integration technique, the computation time needed for evaluating these integrals severely limits the physical dimensions of the antenna problems being analyzed. In this section, a novel approach is introduced by initially approximating the well-behaved transform domain expressions of these integrals, and then performing the inverse transform operations via a set of exact identities [46]. The resulting space domain expressions are valid for a wide range of parameters, with their computation times being comparable to those of the RCM approximation.

Using the following transform pair

$$\tilde{\vec{\Pi}} = \int_{-\infty}^{\infty}\int \vec{\Pi} \exp[-j(\alpha x + \beta y)]\, dx\, dy \tag{43a}$$

$$\vec{\Pi} = \frac{1}{4\pi^2} \int_{-\infty}^{\infty}\int \tilde{\vec{\Pi}} \exp[j(\alpha x + \beta y)]\, d\alpha\, d\beta\ , \tag{43b}$$

one can derive the transform domain expressions for the three vector potential components shown in (9)-(11) in the following forms [43]-[47]:

$$\tilde{{}_0\Pi}_{hx} = \frac{1}{jk_1^2(1-\kappa)} (\gamma_1 - \gamma_2) \exp(-j\gamma_1 z_2) \tag{44}$$

$$\tilde{{}_0\Pi}_{hz} = \frac{j\alpha}{k_1^2\kappa}\left[1 - (\kappa+1)\frac{\gamma_2}{\kappa\gamma_1 + \gamma_2}\right]\exp(-j\gamma_1 z_2) \tag{45}$$

$$\tilde{{}_0\Pi}_{vz} = \frac{\kappa}{j(\kappa\gamma_1 + \gamma_2)} \exp(-j\gamma_1 z_2) \tag{46}$$

where $z_2 = z + h$, and $\gamma_{1,2}$ are explicitly expressed as

$$\gamma_1 = (k_1^2 - \alpha^2 - \beta^2)^{1/2} \quad ; \quad \mathrm{Im}(\gamma_1) \leq 0 \tag{47a}$$

$$\gamma_2 = (\kappa k_1^2 - \alpha^2 - \beta^2)^{1/2} \quad ; \quad \mathrm{Im}(\gamma_2) \leq 0 \quad . \tag{47b}$$

In addition, the free-space Green's function g can also be expressed in the transform domain (see Equation (8)) yielding the following transform pair:

$$\tilde{g}(\alpha,\beta,z_2) = \frac{1}{2j\gamma_1} \exp(-j\gamma_1 z_2) \tag{48a}$$

$$g(x,y,z_2) = \exp(-jk_1 r_2)/4\pi r_2 \quad ; \quad r_2 = [x^2 + y^2 + z_2^2]^{1/2} \quad . \tag{48b}$$

By applying a successive $\partial/\partial z$ operator to (48), an infinite set of transform pairs is obtained, viz.,

$$\tilde{Q}_n = \gamma_1^{n-1} \exp(-j\gamma_1 z_2) \tag{49a}$$

$$Q_n = 2(j)^{n+1} \frac{\partial^n}{\partial z^n} g(x,y,z_2) \quad ; \quad n = 0,1,2,\ldots \tag{49b}$$

where Q is expressed in a closed form for all n and can be numerically evaluated quite rapidly (see the Appendix).

An examination of the Fourier transformed vector potentials in (44)-(46) and the $\tilde{Q}_n$ in (49a) reveals two important and useful properties. First, all of the expressions have an identical z-variation term that corresponds to a space-domain solution emanating at the image point P_2. Second, it is apparent that all of the equations are well-behaved in the Fourier domain and decay exponentially to zero outside the circle $\alpha^2 + \beta^2 = k_1^2$. These properties give rise to the possibility of performing the inverse transform operation on Equations (44)-(46) via the use of the (49) identities. The major obstacle to such a procedure is the existence of γ_2 in these expressions which is overcome in the following section using an appropriate approximation.

5.1 Approximating γ_2 and Space-Domain Results

All three Fourier transform domain expressions in (44)-(46) can be put into the following general form

$$\tilde{\Pi}_0 = f(\gamma_1,\gamma_2) \exp(-j\gamma_1 z_2) \quad . \tag{50}$$

As mentioned before, an important property of Equation (50) is the exponential term which rapidly decays to zero outside the circle $\alpha^2 + \beta^2 = k_1^2$. This fact enables one to replace γ_2, defined in (47b), with the first term of its Taylor series expansion $\bar{\gamma}_2$, that is,

$$\gamma_2 = k_1\sqrt{\kappa}\left[1 - \frac{\alpha^2+\beta^2}{2k_1^2\kappa} - \frac{1}{8}\left(\frac{\alpha^2+\beta^2}{k_1^2\kappa}\right)^2 - \cdots\right] \quad ; \quad \alpha^2+\beta^2 \leq k_1^2|\kappa| \tag{51a}$$

$$\bar{\gamma}_2 = k_1\sqrt{\kappa} \quad . \tag{51b}$$

For most practical values of κ, i.e., $|\kappa| \geq 10$, the approximation in (51b) is excellent inside the circle $\alpha^2 + \beta^2 \leq k_1^2$. Fortunately, the decaying exponential in (50) can easily overcome the errors introduced by (51b) in the region $\alpha^2 + \beta^2 \geq k_1^2$ thereby making this a valid approximation throughout the $\alpha\beta$-plane for a wide range of κ and z_2 parameters, namely,

$$\overset{=}{0\Pi} \simeq f(\gamma_1, \bar{\gamma}_2)\exp(-jk_1z_2) \tag{52}$$

where the bar on the top represents the approximate quantities. It should be noted that Kuo and Mei [29, Eq. 8] have recently verified and used the aforementioned approximation for simplifying the space domain expressions, while Chang et al. [51] have employed an equivalent approximation for representing the vector potential in the vertical current element problem in the terms of an incomplete Hankel function.

Applying the approximation in (52) to the vector potential expressions (44)-(46), and then performing the inverse transform via the aid of the (49) identities, one arrives at the following space domain results [47]:

$$0\bar{\Pi}_{hx} = \frac{-2}{k_1^2(1-\kappa)}\left[jk_1\sqrt{\kappa}\,\frac{\partial}{\partial z}\,g(r_2) + \frac{\partial^2}{\partial z^2}\,g(r_2)\right] \tag{53}$$

$$0\bar{\Pi}_{hz} = \frac{1}{k_1^2\kappa}\left[-2\,\frac{\partial^2}{\partial x\partial z}\,g(r_2) - jc(\kappa+1)\,\frac{\partial}{\partial x}\,S(r_2)\right] \tag{54}$$

$$0\bar{\Pi}_{vz} = S(r_2) \quad , \tag{55}$$

where $c = k_1/\sqrt{\kappa}$ and $S(r_2)$ satisfy the following first-order inhomogeneous linear differential equation:

$$\frac{\partial}{\partial z}\left[S(\rho,z_2)\exp(-jcz_2)\right] = 2\exp(-jcz_2)\,\frac{\partial}{\partial z}\,g(\rho,z_2) \tag{56}$$

where, for convenience, the functional dependences of S and g have been reduced from (x,y,z_2) to (ρ,z_2). By integrating (56) with respect to z_2, and after some algebraic manipulations, the following expression is derived for S:

$$S(\rho,z_2) = [S(\rho,z_2') - 2g(\rho,z_2')] \exp[jc(z_2 - z_2')] + 2g(\rho,z_2)$$
$$+ 2jc \exp(jcz_2) \int_{z_2'}^{z_2} g(\rho,z) \exp(-jcz)\, dz \quad . \tag{57}$$

The secondary height z_2' is an arbitrary starting point needed for obtaining a unique solution to the differential equation (56). Since no simple starting point can be found at which $S(\rho,z_2')$ is known, it is assumed that z_2 is large enough so that the RCM approximation in Equation (39) is applicable (see Figure 9), that is,

$$S(\rho,z_2') = \frac{2\kappa \cos\Theta_2'}{\kappa \cos\Theta_2' + \sqrt{\kappa - \sin^2\Theta_2'}}\, g(\rho,z_2') \tag{58}$$

where angle Θ_2' is defined in Figure 9.

In summary, the three components of the vector potentials are easily solved. The horizontal component (53) is entirely expressed in closed form, while the two vertical components are expressed as integrals. At the point (ρ,z_2), demonstrated in Figure 9, and starting from a higher observation point (ρ,z_2') at which the RCM expressions are valid, (57) is simply used to integrate down to (ρ,z_2). This procedure also effectively computes the correction terms for the RCM approximations of the vertical vector potential components in the region where RCM alone breaks down.

The integration interval in (57), in general, is less than a wavelength long and never intercepts the singularity located at P_2. Also note that the integrand in (57) is independent of z_2', thereby making it possible to generate the vector potential values along the vertical lines z_2z_2' with a single integration by incrementally stepping on the upper limit z_2. As concluded in [47], the above approximations are valid when the following conditions are satisfied:

$$|\kappa| > 5 \tag{59a}$$

$$k_1z_2 > \frac{5}{\sqrt{|\kappa| - 1}} \quad . \tag{59b}$$

Note that Equations (53)-(55) are entirely dependent on various partial derivatives of $g(r_2)$, therefore making E- and H-field approximations dependent on mixed partials of $g(r_1)$ and $g(r_2)$. These derivatives can be rapidly generated on a digital computer using the expansions given in the Appendix.

The approximate formulas are summarized in this section; i.e., Equations (53)-(55) are on the average about five times slower to evaluate numerically than the RCM technique; however, they are about one to two orders of magnitude

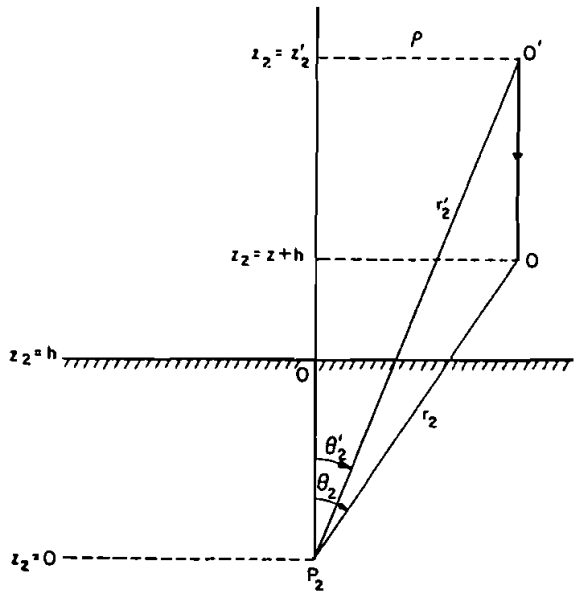

Figure 9. Geometry for computing the vertical vector potential components. r_2' is chosen to be large enough so that the RCM expressions are valid at 0'. Therefore, the vector potential values along the interval 0'0 are obtained by using the initial value at 0' and integrating down along the z-axis.

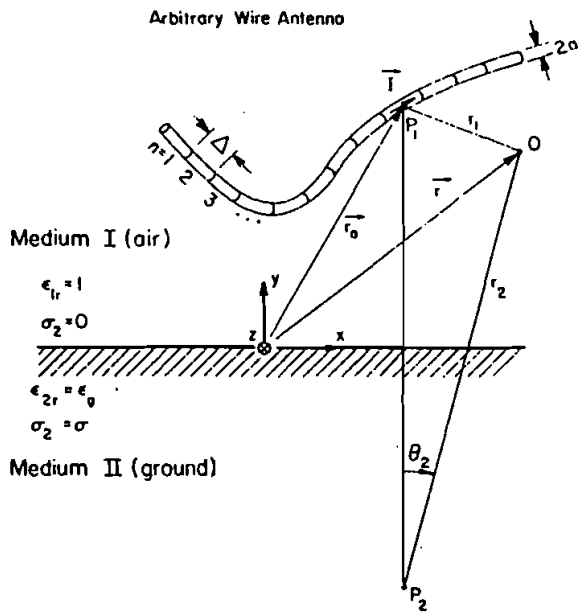

Figure 10. The geometry of an arbitrarily shaped wire antenna located over a lossy half-space.

faster than the reported Sommerfeld integration techniques. As verified by the (59a) and (59b) constraints, the formulas are valid for a wide range of parameters. Table 1 is a comparison of the accuracy of the three techniques in evaluating ${}_0\Pi_{vz}$. Note the consistent superiority of the approximate technique over the RCM approximation for the wide range of parameters tested.

6. WIRE ANTENNAS RADIATING OVER A LOSSY HALF-SPACE

The approximate field solution to the current element problem radiating over a lossy half-space, developed in the previous section in conjunction with the method of moments, can be employed to analyze a wide variety of thin-wire antenna problems radiating over a lossy half-space. Figure 10 depicts the geometry of an arbitrarily shaped wire antenna over a lossy half-space, with (r_a,θ_a,ϕ_a) defining a point on the antenna axis. For simplicity, it is assumed that the antenna is entirely in the xz-plane ($\phi_a = 0$).

Assuming that the antenna is excited by the field $\vec{E}^{exc}(\vec{r}_a)$, and has a loading function $\Lambda(\vec{r}_a)$ ohms/meter, one can write a general integral equation enforcing the total E-field along the antenna equal to that induced by the antenna loading, that is,

$$\hat{I}(\vec{r}_a) \cdot \vec{e}^{exc}(\vec{r}_a) + \hat{I}(\vec{r}_a) \cdot \int_{antenna} [\vec{G}_v(\vec{r}_a,\vec{r}_a')\hat{z} \cdot \hat{I}(\vec{r}_a') + \vec{G}_H(\vec{r}_a,\vec{r}_a')\hat{x} \cdot \hat{I}(\vec{r}_a')]dr_a'$$

$$= \Lambda(\vec{r}_a)\hat{I}(\vec{r}_a) \quad , \tag{60}$$

where $\hat{I}(\vec{r}_a)$ is a unit vector along the antenna direction and the kernels $\vec{G}_v(\vec{r}_a,\vec{r}_a')$ and $\vec{G}_h(\vec{r}_a,\vec{r}_a')$ are the E-fields induced at point $\vec{r}_a$ due to a one-ampere electric current element located at $\vec{r}_a'$ and oriented in the z- and the x-directions, respectively. As shown in [47], G_v and G_h are simply related to the vector potentials via some differentiations.

As developed by Harrington [50], [52], the method of moments is a convenient technique for transforming the antenna integral equation into a numerically manageable matrix form. In this work, pulse-basis and delta-matching functions are chosen since they eliminate the need for integrating the kernels $\vec{G}_v$ and $\vec{G}_h$. A finite difference [53]-[54] algorithm is used to generate the differential operators. The number of unknown patches on the antenna N should be large enough so that the patch Δ is at least 1/6 of the wavelength. Discarding all of the details here, a general computer program is written [47] to generate the current distribution and the far-field patterns of an arbitrarily shaped wire antenna over a lossy half-space. Also, programs are developed to determine the transient response of the antenna [43]-[44]. In this section, we only present a few representative numerical results from [55]. The horizontal antenna shown in Figure 11 is the first example. Fortunately, because of the symmetries present in this geometry, the $[Z^{imp}]$ matrix is in a Toeplitz matrix form. Therefore, one needs to compute only one row of this matrix and use the aforementioned symmetry to complete it. Figures 12 and 13 are generated to show the radiation patterns of the 2L = 10 meters center-fed antenna

Table 1. Comparison of the RCM, exact, and the approximate evaluations of ${}_0\Pi_{vz}$. For this example, f = 30 MHz, $\theta_2 = 45°$ and $\phi_2 = 0°$.

	$k_1 r_2$	$k_1 z_2$	Min. $k_1 z_2$ Eq.(59b)	RCM value x 10^2	Exact integration x 10^2	Approximate technique x 10^2
ε_g=5, σ=.001, $\lvert\kappa\rvert$=5.04	.1	.07	2.49	62.1-j7.49	79.6-j11.2	96.3-j17.2
	1.	.71	2.49	3.28-j5.33	3.22-j6.52	2.94-j7.13
	2.	1.41	2.49	-1.36-j2.82	-1.84-j2.95	-1.96-j2.88
	6.	4.24	2.49	1.01+j2.72	1.06+j2.00	1.03-j2.09
	10.	7.07	2.49	-.518+j.351	-.507+j.383	-.518+j.351
ε_g=10, σ=.01, $\lvert\kappa\rvert$=11.7	.1	.07	1.53	70.5-j12.4	90.8-j15.8	96.6-j15.7
	1.	.71	1.53	3.41-j6.30	3.47-j7.76	3.42-j7.86
	2.	1.41	1.53	-1.73-j3.14	-2.23-j3.34	-2.28-j3.30
	6.	4.24	1.53	1.17+j.247	1.23+j.184	1.19+j.179
	10.	7.07	1.53	-.570+j.433	-.562+j.465	-.570+j.433
ε_g=40, σ=1, $\lvert\kappa\rvert$=601	.1	.07	.204	95.0-j13.2	99.5-j11.0	99.6-j11.0
	1.	.71	.204	4.87-j8.26	5.09-j8.52	5.09-j8.52
	2.	1.41	.204	-2.16-j4.28	-2.22-j4.39	-2.22-j4.40
	6.	4.24	.204	1.55+j.388	1.57+j.386	1.57+j.386
	10.	7.07	.204	-.784+j.552	-.788+j.560	-.784+j.552

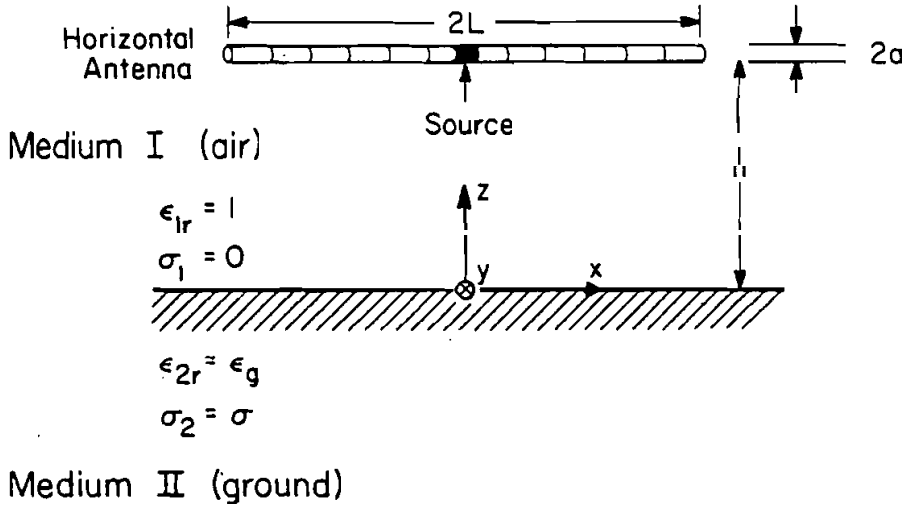

Figure 11. Center-fed horizontal dipole over a lossy half-space.

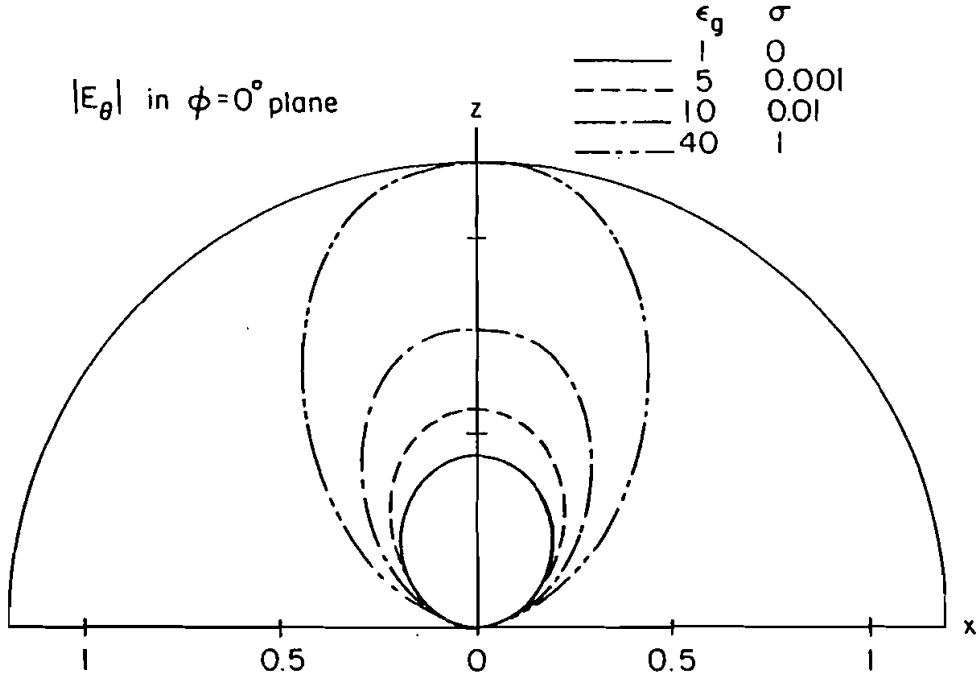

Figure 12. Far-field radiation pattern for the horizontal antenna at 15 MHz and constant gap voltage. Note that the patterns are computed at $k_1 r = 500$, and in this plane, $|E_\phi|$ is negligible.

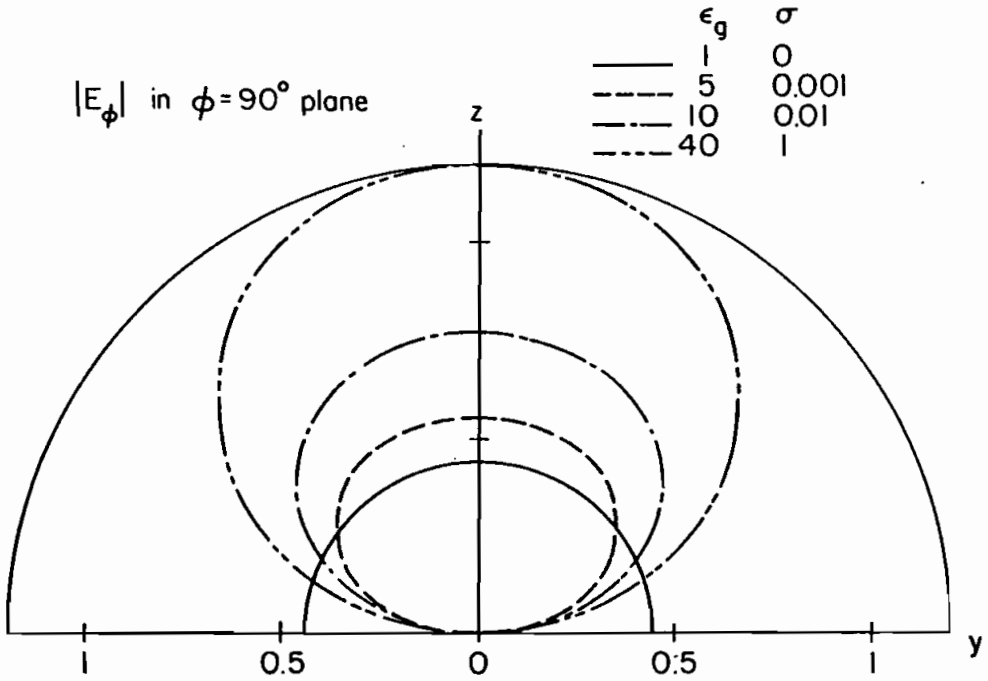

Figure 13. Far-field radiation pattern for the horizontal antenna at 15 MHz and constant gap voltage. Note that the patterns are computed at $k_1 r = 500$, and in this plane, $|E_\theta|$ is negligible.

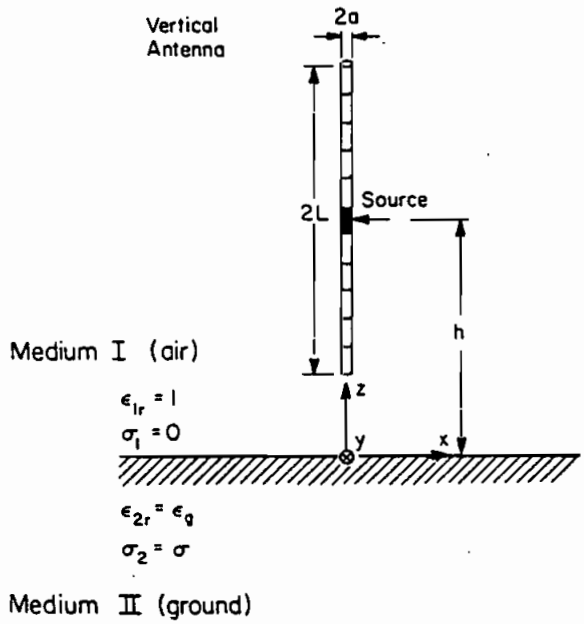

Figure 14. Center-fed vertical dipole over a lossy half-space.

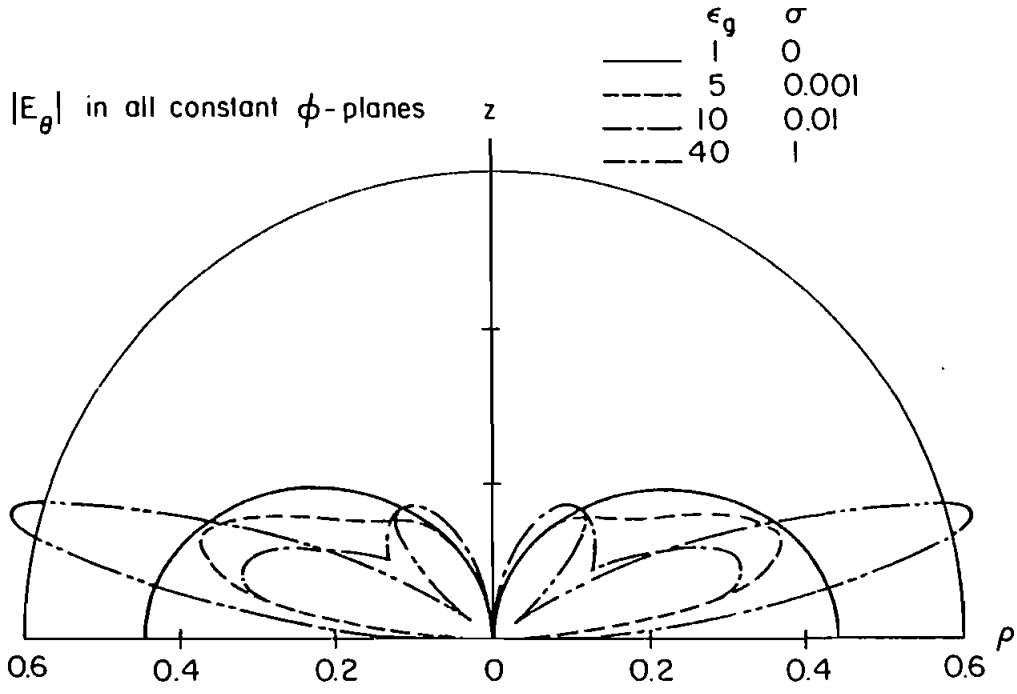

Figure 15. The far-field radiation pattern for a center-fed vertical dipole (2L = 10m, h = 8m, and 2a = 0.1m) at 15 MHz and constant gap voltage. Note that the patterns are computed at $k_1 r = 500$, and in this example, $|E_\phi|$ is negligible.

at 15 MHz. The vertical dipole shown in Figure 14 is the next geometry considered. Unfortunately, as was the case for the horizontal antenna, the total $[Z^{imp}]$ matrix is not in a Toeplitz form. However, the computer program is designed to take maximum advantage of the available symmetry. As an example, Figure 15 is included to show the radiation pattern of a 2L = 10 meters, h = 8 meters, center-fed vertical dipole (f = 15 MHz) located over various lossy grounds.

APPENDIX: VARIOUS PARTIAL DERIVATIVES OF g

The free-space Green's function g, which is defined as

$$g = g(x_1,x_2,x_3) = \exp(-jkr)/4\pi r \quad ; \quad r = [x_1^2 + x_2^2 + x_3^2]^{1/2} \quad , \qquad (A.1)$$

is singular only at the point r = 0; therefore, its partial derivatives exist for all r > 0 and can be represented in a closed form. In order to express these derivatives in an organized manner and suitable for numerical evaluation, the auxiliary function R_i is introduced as

$$R_i = (-1)^i\{1 \times 2 \times 4 \times \ldots \times (2i - 2) + jkr[1 \times 3 \times 5 \times \ldots \times (2i - 3)]\}r^{-2i}$$

$$i = 1,2,3, \ldots \qquad (A.2)$$

where R_i has the following convenient property

$$\frac{\partial}{\partial x_j} R_i = x_j R_{i+1} \quad ; \quad i = 1,2, \ldots \quad ; \quad j = 1,2,3 \quad . \tag{A.3}$$

The various partial derivatives of g can now be expressed in terms of x_j, R_2, and lower-order partials of g.

a) Partial derivatives of one variable

$$\frac{\partial}{\partial x_j} g = x_j R_1 g \tag{A.4}$$

$$\frac{\partial^2}{\partial x_j^2} g = (R_1 + x_j^2 R_2) g + x_j R_1 \frac{\partial}{\partial x_j} g \tag{A.5}$$

$$\frac{\partial^3}{\partial x_j^3} g = (3x_j R_2 + x_j^3 R_3) g + 2(R_1 + x_j^2 R_2) \frac{\partial}{\partial x_j} g + x_j R_1 \frac{\partial^2}{\partial x_j^2} g \tag{A.6}$$

. . .
. . .

where j = 1,2,3 holds for Equations (A.4) - (A.6).

b) Mixed partial derivatives of two variables

$$\frac{\partial^2}{\partial x_j \partial x_k} g = x_j x_k R_2 g + x_k R_1 \frac{\partial}{\partial x_j} g = x_j x_k (R_1^2 + R_2) g \tag{A.7}$$

$$\frac{\partial^3}{\partial x_j^2 \partial x_k} g = x_k (R_2 + x_j^2 R_3) g + 2x_j x_k R_2 \frac{\partial}{\partial x_j} g + x_k R_1 \frac{\partial^2}{\partial x_j^2} g \tag{A.8}$$

$$\frac{\partial^4}{\partial x_j^3 \partial x_k} g = x_k (3x_j R_3 + x_j^3 R_4) g + 3x_k (R_2 + x_j^2 R_3) \frac{\partial}{\partial x_j} g + 3x_j x_k R_2 \frac{\partial^2}{\partial x_j^2} g + x_k R_1 \frac{\partial^3}{\partial x_j} g \tag{A.9}$$

$$\frac{\partial^4}{\partial x_j^2 \partial x_k^2} g = [R_2 + (x_j^2 + x_k^2) R_3 + x_j^2 x_k^2 R_4] g + x_k (R_2 + x_j^2 R_3) \frac{\partial}{\partial x_k} g + 2x_j (R_2 + x_k^2 R_3) \frac{\partial}{\partial x_j} g + (R_1 + x_k^2 R_2) \frac{\partial^2}{\partial x_j^2} g + 2x_j x_k R_2 \frac{\partial^2}{\partial x_j \partial x_k} g + x_k R_1 \frac{\partial^3}{\partial x_j^2 \partial x_k} g \tag{A.10}$$

. . .
. . .

where $j \neq k$ and j,k = 1,2,3 assumed for Equations (A.7) and (A.10).

c) Mixed partial derivatives of three variables

$$\frac{\partial^3}{\partial x_j\,\partial x_k\,\partial x_\ell} g = x_j x_k x_\ell R_3 g + 2x_k x_\ell R_2 \frac{\partial}{\partial x_j} g + x_\ell R_1 \frac{\partial^2}{\partial x_j\,\partial x_k} g \tag{A.11}$$

$$\frac{\partial^4}{\partial x_j^2\,\partial x_k\,\partial x_\ell} g = x_k x_\ell (R_3 + x_j^2 R_4) g + 3x_j x_k x_\ell R_3 \frac{\partial}{\partial x_j} g + 2x_k x_\ell R_2 \frac{\partial^2}{\partial x_j^2} g + x_j x_\ell R_2 \frac{\partial^2}{\partial x_j\,\partial x_k} g + x_\ell R_1 \frac{\partial^3}{\partial x_j^2\,\partial x_k} g \tag{A.12}$$

. . .
. . .

where $j \neq k \neq \ell$ and $j,k,\ell = 1,2,3$ are assumed for Equations (A.11) and (A.12).

REFERENCES

[1] A. Baños, Dipole Radiation in the Presence of a Conducting Half-Space. Oxford: Pergamon Press, 1966.

[2] E. F. Kuester and D. C. Chang, "Evaluation of Sommerfeld integrals associated with dipole sources above the earth," University of Colorado, Scientific Report 43, Jan. 1979.

[3] A. Sommerfeld, "Uber die Ausbreitung der Wellen in der drahtlosen Telegraphie," Annalen der Physik (4th Folge), vol. 28, pp. 665-736, 1909.

[4] A. Sommerfeld, "Uber die Ausbreitung der Wellen in der drahtlosen Telegraphie," Annalen der Physik (4th Folge), vol. 81, pp. 1135-1153, 1926.

[5] V. A. Fock, "Zur Berechnung des elektromagnetischen Wechselstromfeldes bie ebener Begrenzung," Annalen der Physik (5th Folge), vol. 17, pp. 401-420, 1933.

[6] V. A. Fock and V. R. Bursian, "Electromagnetic field of alternating currents in a circuit grounded at both ends," Zh. Russk. Fiz.-Khim. Obshch. (Chast' Fizich.), vol. 58, pp. 355-363 [Russian], 1926.

[7] W. H. Wise, "Asymptotic dipole radiation formulas," Bell Syst. Tech. J., vol. 8, pp. 662-671, 1929.

[8] W. H. Wise, "The grounded condenser antenna radiation formula," Proc. IRE, vol. 19, pp. 1684-1689, 1931.

[9] S. O. Rice, "Series for the wave function of a radiating dipole at the earth's surface," Bell Syst. Tech. J., vol. 16, pp. 101-109, 1937.

[10] P. A. Ryazin, "Propagation of radio waves near the earth's surface," Trudy Fiz. Inst. P.N. Lebedev, vol. 3, vyp. 2, pp. 45-120, [Russian], 1946.

[11] B. Van der Pol, "Theory of the reflection of the light from a point source by a finitely conducting flat mirror, with an application to radiotelegraphy," Physica, vol. 2, pp. 843-853, 1935. Also in Van der Pol, Selected Scientific Papers, vol. 2. Amsterdam: North-Holland, pp. 857-867, 1960.

[12] L. H. Thomas, "A transformation of a formula of Sommerfeld," Proc. Cambridge Phil. Soc., vol. 26, pp. 123-126, 1930.

[13] M. M. Agrest and M. S. Maksimov, Theory of Incomplete Cylindrical Functions and Their Applications. Berlin: Springer-Verlag, 1971, p. 330.

[14] J. R. Wait, "The electromagnetic fields of a horizontal dipole in the presence of a conducting half-space," Can. J. Phys., vol. 39, pp. 1017-1028, 1961.

[15] J. R. Wait, Electromagnetic Waves in Stratified Media. Oxford: Pergamon Press, 1970, p. 608.

[16] J. R. Wait and J. A. Fuller, "On radio propagation through earth," IEEE Trans. Antennas Propagat., vol. 18, pp. 796-798, 1971.

[17] L. V. Kochmanova and V. P. Perov, "Power dissipated in dipole excitation of an electromagnetic field above a conducting half-space," Radiotekh. Elektron., vol. 19, pp. 1832-1838 [Russian] = Radio Eng. Electron. Phys., vol. 19, no. 9, 17-23, 1974.

[18] N. Bleistein and R. A. Handelsman, Asymptotic Expansions of Integrals. New York: Holt, Rinehart and Winston, 1975, p. 425.

[19] L. M. Brekhovskish, Waves in Layered Media. New York: Academic Press, 1960, p. 561.

[20] K. G. Budden, Radio Waves in the Ionosphere. Cambridge: University Press, 1966, p. 542.

[21] L. B. Felsen and N. Marcuvitz, Radiation and Scattering of Waves. Englewood Cliffs, N.J.: Prentice-Hall, 1973, p. 888.

[22] A. Yokoyama, "Dipole radiation effected by the plane earth," J. Phys. Soc. Japan, vol. 27, pp. 224-229, 1969.

[23] A. Yokoyama, "Radiation of a dipole in a lossy half-space," J. Phys. Soc. Japan, vol. 32, pp. 270-278, 1972.

[24] A. Yokoyama, "Comments on the solutions of dipoles in semi-infinite media," IEEE Trans. Antennas Propagat., vol. 22, pp. 339-340, 1974.

[25] O. A. Aboul-Atta, L. Shafai and M. Z. Tarnawecky, "Electromagnetic earth induction from an overhead line current parallel to the ground," URSI Digest, University of Laval, Quebec, Canada, p. 77, 1980.

[26] P. J. T. Philippi and D. Habault, "Reflexion of a spherical wave by the plane interface between a perfect fluid and a porous medium," J. Sound Vib., vol. 56, pp. 97-103, 1978.

[27] G. N. Krylov, "Structures of electromagnetic fields of directional antennas above a flat earth with finite conductivity," Radiotekh. Elektron., vol. 6, pp. 747-753 [Russian] = Radio Eng. Electron. Phys., vol. 6, pp. 660-666, 1961.

[28] J. N. Brittingham, E. K. Miller and J. T. Okada, "SOMINT: An improved model for studying conducting objects near lossy half-spaces," Rept. No. UCRL-52423, Lawrence Livermore Lab., Univ. of California, Livermore, Calif., 1978.

[29] W. C. Kuo and K. K. Mei, "Numerical approximations of the Sommerfeld integral for fast convergence," Radio Science, vol. 13, pp. 407-415, 1978.

[30] D. C. Chang and J. R. Wait, "Appraisal of near-field solutions for a Hertzian dipole over a conducting half-space," Can. J. Phys., vol. 48, pp. 737-743, 1970.

[31] M. Siegel and R. W. P. King, "Electromagnetic fields in a dissipative half-space: a numerical approach," J. Appl. Phys., vol. 41, pp. 2415-2423, 1970.

[32] E. K. Miller, A. J. Poggio, G. J. Burke and E. S. Selden, "Analysis of wire antennas in the presence of a conducting half-space: Part I. The vertical antenna in free space," Can. J. Phys., vol. 50, pp. 879-888, 1972.

[33] E. K. Miller, A. J. Poggio, G. J. Burke and E. S. Selden, "Analysis of wire antennas in the presence of a conducting half-space: Part II: The horizontal antenna in free space," Can. J. Phys., vol. 50, pp. 2614-2627, 1972.

[34] J. A. Kong, L. C. Shen and L. Tsang, "Field of an antenna submerged in a dissipative dielectric medium," IEEE Trans. Antennas Propagat., vol. 25, pp. 887-889, 1977.

[35] R. W. P. King and B. Sandler, "Subsurface communications between dipoles in general media," IEEE Trans. Antennas Propagat., vol. 25, pp. 770-775, 1977.

[36] R. J. Lytle and D. L. Lager, "Numerical evaluation of Sommerfeld integrals," Rept. No. UCRL-51688, Lawrence Livermore Lab., Univ. of California, Livermore, Calif., 1974.

[37] J. R. Wait and J. A. Fuller, "On radio propagation through earth," IEEE Trans. Antennas Propagat., vol. 18, pp. 796-798, 1971.

[38] H. A. Haddad and D. C. Chang, "Field computation of an arbitrarily-oriented dipole above a layered earth," Sci. Rept. No. 22, Electromagnetics Laboratory, Dept. of Elect. Eng., Univ. of Colorado, Boulder, CO, 1977.

[39] T. K. Sarkar, "Analysis of arbitrarily oriented thin wire antennas over a plane imperfect ground," Arch. Elek. Übertrangungstech., vol. 31, pp. 449-457, 1977.

[40] J. D. McCannon, "A comparative numerical study of several methods for analyzing a vertical thin-wire antenna over a lossy half-space," Ph.D. Thesis, University of Illinois, Urbana, Illinois, 1974.

[41] J. N. Brittingham, E. K. Miller and J. T. Okada, "Bivariate interpolation approach for efficiently and accurately modelling antennas over a half-space," Electron. Lett., vol. 13, pp. 690-691, Nov. 1977.

[42] Y. Rahmat-Samii, P. Parhami and R. Mittra, "An alternative approach for an efficient and accurate evaluation of Sommerfeld integrals," AP-S Internat. Symp. Proceedings, Amherst, Mass., pp. 147-150, 1978.

[43] Y. Rahmat-Samii, P. Parhami and R. Mittra, "Transient response of a loaded horizontal antenna over lossy ground with application to EMP simulators," University of Illinois at Urbana-Champaign, Electromagnetics Laboratory Report No. 77-26, Dec. 1977.

[44] Y. Rahmat-Samii, P. Parhami and R. Mittra, "Loaded horizontal antenna over an imperfect ground," IEEE Trans. Antennas Propagat., vol. AP-26, no. 6, pp. 789-796, Nov. 1978.

[45] P. Parhami, Y. Rahmat-Samii and R. Mittra, "An efficient approach for evaluating the Sommerfeld integrals encountered in the current element radiating over lossy ground," IEEE Trans. Antennas Propagat., vol. 28, pp. 100-104, Jan. 1980.

[46] R. Mittra, P. Parhami and Y. Rahmat-Samii, "Solving current element problems over lossy half-space without Sommerfeld integrals," IEEE Trans. Antennas Propagat., vol. 27, pp. 778-782, Nov. 1979.

[47] P. Parhami, "Analysis of arbitrarily shaped wire antennas radiating over a lossy half-space," Ph.D. Thesis, University of Illinois, Urbana, Illinois, 1979.

[48] Y. Rahmat-Samii and R. Mittra, "Spectral analysis of high frequency diffraction of an arbitrary incident field by a half-plane -- Comparison with four asymptotic techniques," Radio Sci., vol. 13, pp. 31-48, Jan./Feb. 1978.

[49] J. A. Kong, Theory of Electromagnetics Waves. New York: Wiley, 1975.

[50] R. F. Harrington, Field Computation by Moment Methods. New York: McMillan, 1968.

[51] D. C. Chang and R. Fisher, "A unified theory on radiation of a vertical electric dipole above a dissipative earth," Radio Sci., vol. 9, no. 12, pp. 1129-1138, Dec. 1974.

[52] R. F. Harrington, "Matrix methods for field problems," Proc. IEEE, pp. 136-149, Feb. 1967.

[53] R. Mittra and W. L. Ko, "A finite difference approach to the wire junction problem," IEEE Trans. Antennas Propagat., vol. AP-23, pp. 435-438, May 1975.

[54] P. Parhami, Y. Rahmat-Samii and R. Mittra, "A technique for calculating the radiation and scattering characteristics of antennas mounted on a finite ground plate," Proc. IEE, vol. 124, pp. 1009-1016, Nov. 1977.

[55] P. Parhami and R. Mittra, "Wire antenna over lossy half space," IEEE Trans. Antennas Propagat., vol. AP-28, pp. 397-403, May 1980.